

Fluid dynamical description of relativistic nuclear collisions

J. R. Nix and D. Strottman

Theoretical Division, Los Alamos National Laboratory  
Los Alamos, New Mexico 87545

Abstract

On the basis of both a conventional relativistic nuclear fluid dynamical model and a two-fluid generalization that takes into account the interpenetration of the target and projectile upon contact, we calculate collisions between heavy nuclei moving at relativistic speeds. This is done by solving the relevant equations of motion numerically in three spatial dimensions by use of particle-in-cell finite-difference computing techniques. We study the effect of incorporating a density isomer, or quasistable state, in the nuclear equation of state at three times normal nuclear density, as well as the effect of doubling the nuclear compressibility coefficient. For the reaction  $^{20}\text{Ne} + ^{238}\text{U}$  at a laboratory bombarding energy per nucleon of 393 MeV, the calculated distributions in energy and angle of outgoing charged particles are compared with recent experimental data both integrated over all impact parameters and for nearly central collisions.

Introduction

Our colloquium on drops and bubbles has brought together people in such diverse disciplines as astrophysics, fluid dynamics, and nuclear physics, working with physical systems ranging in size from stars through water drops to atomic nuclei. Having already heard from astrophysicists and fluid dynamicists, it is time now to turn our attention from some of the largest objects in the universe to some of the smallest.

An atomic nucleus, with diameter about  $10^{-14}$  m and mass about  $10^{-25}$  kg, is about  $10^4$  times as dense as water. Discovered in 1911 by Sir Ernest Rutherford, it is to lowest order a collection of positively charged protons and uncharged neutrons held tightly together by short-range nuclear forces. As first suggested by Niels Bohr in 1936, a nucleus behaves in some respects like a uniformly charged drop of liquid with surface tension.

The liquid-drop model has been widely used to explain the breakup of a heavy nucleus into two smaller fragments in the process of nuclear fission, as well as to explain many features associated with collisions between two nuclei. Until recently, the bombarding energy in such collisions has been fairly low, with the result that the nuclear density remains close to its equilibrium value and the excitation energy is relatively low. However, a few years ago accelerators were developed that can accelerate heavy nuclei to relativistic speeds, and we are now beginning to explore what happens when nuclei become highly compressed and excited.

The collision of heavy nuclei at high energy is extremely complicated, lying somewhere in between two limiting possibilities that have been used to describe it. At one extreme, the process could be dominated by a series of collisions between individual particles making up the nuclei or produced in the reaction. This first limit, which would be realized if the particle mean free path were much longer than the nuclear force range, has been studied in terms of microscopic approaches such as the relativistic intranuclear cascade, where the basic input is experimentally measured two-particle cross sections.<sup>1-3</sup>

At the other extreme, the process could be dominated by coherent collective-field effects, resembling instead the collision of two drops of nuclear fluid. This second limit would be realized if there are many degrees of freedom, sufficient time during the collision to establish local equilibrium, and a short mean free path for stopping a particle. In relativistic nuclear collisions of the type considered here, the first two conditions are satisfied moderately well whereas the last condition is more uncertain. Estimates based on collisions between two particles in free space give relatively long mean free paths, but the mean free path could be reduced significantly inside a nuclear medium because of many-body effects or a nuclear phase transition.<sup>4</sup> This second limit has been studied by several different groups around the world in terms of fluid dynamical models, where the basic input is the nuclear equation of state. We will be concentrating here on recent work performed at Los Alamos within this approach.<sup>5-7</sup>

### Nuclear equation of state

One reason for studying relativistic nuclear collisions is to learn about the nuclear equation of state, the fundamental relationship specifying how pressure depends upon density and thermal energy. At present we have experimental information about this important function only in the vicinity of the equilibrium ground state. However, theoretical speculations suggest that it may be extremely complicated, with nuclear matter undergoing one or more phase transitions as its density is increased.<sup>5</sup> This is illustrated schematically in Figure 1, which shows how the ground-state energy per nucleon  $E_0(n)$ , or zero-temperature compressional energy per nucleon, might depend upon nucleon number density  $n$ . We know experimentally that the equilibrium energy per nucleon  $E_0(n_0) = -16$  MeV, that the equilibrium density  $n_0 = 1.5 \times 10^{14}$  nucleons/m<sup>3</sup>, and that the nuclear compressibility coefficient  $K = 210$  MeV. What happens away from equilibrium is currently unknown, but doubling the nuclear density from its normal value could lead to a pion condensate, or a state containing a large number of bound pions. Compression to several times normal density could result in a density isomer, or a quasistable state existing at other than normal density. Still further compression could produce quark matter, in which the quarks that comprise nucleons become free. To determine whether or not any of these phase transitions actually exist in nuclei is the exciting challenge that we face!

In addition to the above compressional energy, nuclear matter at rest can contain thermal energy, so that the total internal energy per nucleon is

$$E(n, I) = E_0(n) + I, \quad (1)$$

where  $I$  is the thermal energy per nucleon, which is itself a function of  $n$  and either the entropy per nucleon  $S$  or the temperature  $T$ . The pressure  $p$  is then given by<sup>5-7</sup>

$$p = n^2 \left. \frac{\partial E(n, I)}{\partial n} \right|_S = n^2 \frac{dE_0(n)}{dn} + n^2 \left. \frac{\partial I}{\partial n} \right|_S, \quad (2)$$

containing separate contributions from the compressional energy and the thermal energy.

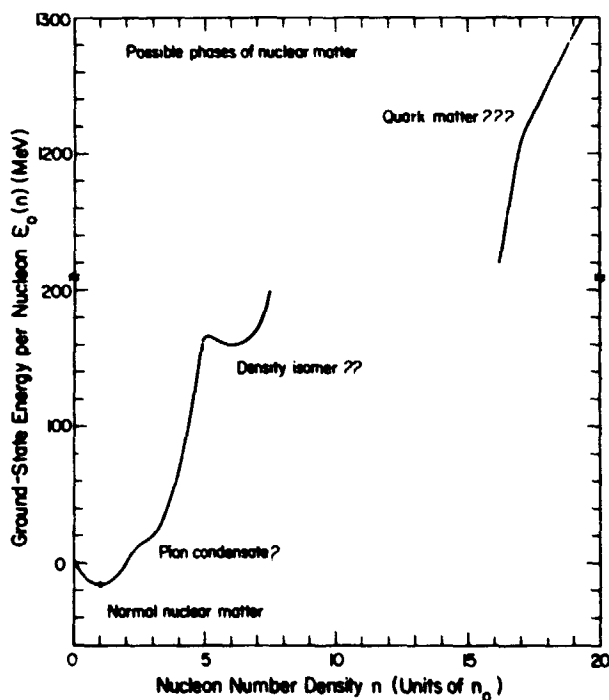


Figure 1. Compressional energy, illustrating three conjectured nuclear phase transitions.

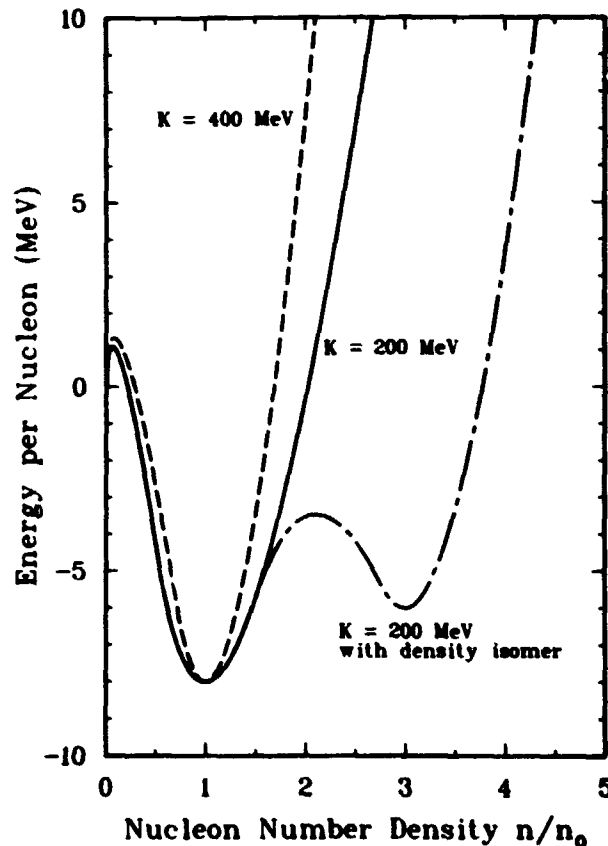


Figure 2. Compressional energy in three of our nuclear equations of state.

For the ground-state energy per nucleon  $E_0(n)$  we use both an old functional form<sup>6</sup>

$$E_0(n) = a n^{2/3} - b n + c n^{5/3} \quad , \quad (3)$$

with positive constants  $a$ ,  $b$ , and  $c$  that yield a compressibility coefficient  $K = 294.8$  MeV, and a new functional form<sup>7</sup> producing the three curves shown in Figure 2. The solid line shows the result for compressibility coefficient  $K = 200$  MeV, and the dashed line shows the effect of doubling the compressibility coefficient to 400 MeV. The dot-dashed curve shows the result for a density isomer at a density that is three times normal nuclear density, with an energy 2 MeV higher than at normal density and with the same curvature. In each of these three cases we use the value  $E_0(n_0) = -8$  MeV to simulate the loss in binding energy for finite nuclei arising from surface and Coulomb energies. The new functional form has the property that the speed of sound approaches the speed of light in the limit of infinite compression. This is achieved by parametrizing  $E_0(n)$  for  $n$  greater than a critical value in terms of three smoothly joined parabolas in the square root of the density, so that in the limit of infinite compression it increases linearly with density.

For the thermal contribution to the pressure we use the result<sup>5-7</sup>

$$P_{\text{thermal}} = n^2 \left. \frac{\partial I}{\partial n} \right|_S = \frac{2}{3} n I \quad , \quad (4)$$

which is derived from the nonrelativistic Fermi-gas model.

#### Relativistic nuclear fluid dynamics

In a complete nuclear fluid dynamical calculation, we would need to take into account nuclear energy, Coulomb energy, nuclear viscosity, thermal conductivity, and single-particle effects, as well as the production of additional particles and the associated radiative loss of energy from the system. However, in nuclear collisions of the type considered here, these effects are small compared to those caused by the dominant kinetic, compressional, and thermal energies, and are consequently neglected.

The covariant relativistic fluid dynamical equations that we solve express the conservation of nucleon number, momentum, and energy, for a specified nuclear equation of state. In units in which the speed of light  $c = 1$ , these equations are<sup>5-7</sup>

$$\frac{\partial N}{\partial t} + \nabla \cdot (\vec{v}N) = 0 \quad , \quad (5)$$

$$\frac{\partial \vec{M}}{\partial t} + \nabla \cdot (\vec{v}\vec{M}) = -\nabla p \quad , \quad (6)$$

and

$$\frac{\partial E}{\partial t} + \nabla \cdot (\vec{v}E) = -\nabla \cdot (\vec{v}p) \quad , \quad (7)$$

where  $N$ ,  $\vec{M}$ , and  $E$  are respectively the nucleon number density, momentum density, and energy density (including rest energy) in the laboratory reference frame and  $\vec{v}$  is the velocity of matter relative to the laboratory frame. The three laboratory-frame quantities are related to rest-frame quantities by

$$N = \gamma n, \quad (8)$$

$$\vec{M} = \gamma^2 (\epsilon + p) \vec{v} \quad , \quad (9)$$

and

$$E = \gamma^2 (\epsilon + p) - p \quad , \quad (10)$$

where  $\gamma = (1 - v^2)^{-1/2}$  and  $\epsilon$  is the internal energy density in the rest frame, which is related to the internal energy per nucleon of Eq. (1) by

$$\epsilon = [m_0 + E(n, I)] n \quad , \quad (11)$$

including the nucleon mass  $m_0$ .

For a given nuclear equation of state and for given initial conditions, we solve these equations numerically in three spatial dimensions by use of a particle-in-cell finite-difference computing method.<sup>5-8</sup> In this technique, the fluid is represented by discrete Lagrangian computational particles, which move through a mesh consisting of fixed cubical Eulerian cells. From finite-difference representations of Eqs. (5)-(7), the values of  $N$ ,  $M$ , and  $E$  for each cell are calculated at later times in terms of preceding values. The values of  $n$ ,  $v$ ,  $\epsilon$ , and  $p$  throughout the mesh are obtained by means of a partial algebraic reduction followed by the iterative solution of a transcendental equation in one unknown.

Some examples of the solutions are shown in Figure 3 for the reaction  $^{20}\text{Ne} + ^{238}\text{U}$  at a laboratory bombarding energy per nucleon of 250 MeV, corresponding to an incident speed that is 62% the speed of light. The nuclear equation of state is given by Eqs. (2)-(4). Each column presents a side view of the matter distribution evolving in time for a different impact parameter. The initial frame in each case shows a  $^{238}\text{U}$  target bombarded from above by a Lorentz-contracted  $^{20}\text{Ne}$  projectile. The projectile and target are represented by computational particles, which are initially aligned so that in the direction perpendicular to the page only a single point is visible. However, as the impulse resulting from the collision propagates throughout the system this alignment is destroyed and additional particles come into view.

The characteristic features of the time evolution vary systematically with impact parameter. In nearly central collisions the target and projectile are substantially deformed, compressed, and excited, with curved shock waves produced. These are followed by rarefaction waves and an overall expansion of the matter into a moderately wide distribution of angles. At the other extreme, in peripheral collisions the projectile is fragmented into a portion that proceeds roughly straight ahead at its original velocity and another portion that deposits its energy in the target. This disturbs the target much less violently than in nearly central collisions, and its deformation, compression, and excitation are therefore much less.

We show in Figure 4 the effect of varying the nuclear equation of state on nearly central collisions at the higher laboratory bombarding energy per nucleon of 393 MeV, corresponding to an incident speed that is 71% the speed of light. The results for the different equations of state are very similar to one another, but for our equation of state with a density isomer the expansion starts somewhat later because the matter is compressed to a higher density than for our two conventional equations of state.

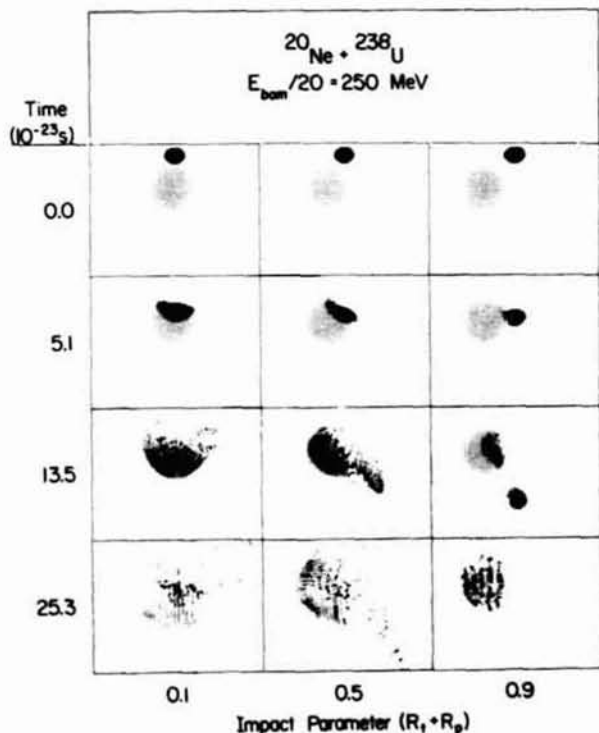


Figure 3. Time evolution of the matter distribution for three impact parameters.

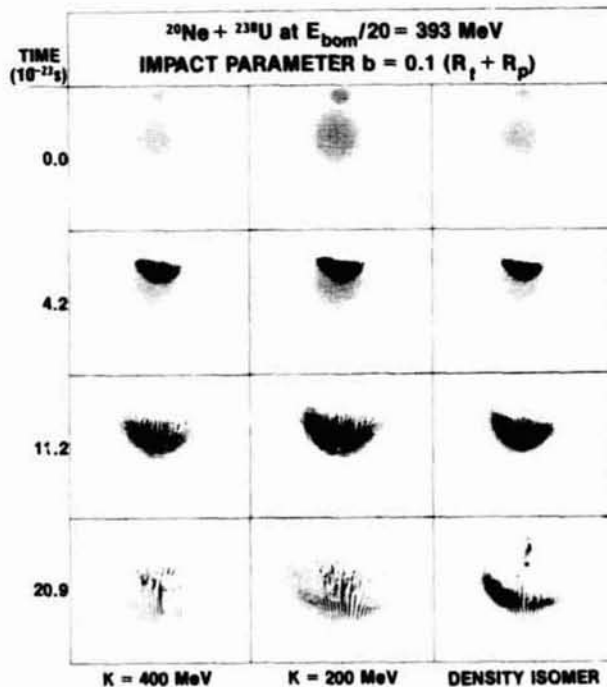


Figure 4. Time evolution of the matter distribution for three nuclear equations of state.

For our conventional equation of state with compressibility coefficient  $K = 200$  MeV, the matter is compressed to a maximum rest-frame density of  $3.9 n_0$  and remains above  $2 n_0$  for  $1.0 \times 10^{-22}$  s. For our stiffer equation of state with  $K = 400$  MeV the matter is compressed to a maximum rest-frame density of  $3.4 n_0$  and remains above  $2 n_0$  for  $0.7 \times 10^{-22}$  s. For our softer equation of state with a density isomer the matter is compressed to a maximum rest-frame density of  $5.1 n_0$  and remains above  $3 n_0$  for  $1.4 \times 10^{-22}$  s and above  $2 n_0$  for  $1.9 \times 10^{-22}$  s.

#### Comparison with experimental data

For the reaction  $^{20}\text{Ne} + ^{238}\text{U}$  at a laboratory bombarding energy per nucleon of 393 MeV, Sandoval et al.<sup>9</sup> have recently measured at the Berkeley Bevalac the distributions in energy and angle of outgoing charged particles, including contributions from protons, deuterons, tritons,  $^3\text{He}$  particles, and  $^4\text{He}$  particles. Also, by selecting only those events containing large numbers of associated charged particles, Stock et al.<sup>10</sup> have measured for nearly central collisions the distributions in energy and angle of outgoing charged particles, including contributions from protons, deuterons, and tritons. Unfortunately, this selection does not eliminate possible contributions from large impact parameters, for which the high-energy yield in forward directions is larger than for central collisions. These experimental data in the form of energy spectra at four laboratory angles ranging from  $30^\circ$  to  $150^\circ$  are shown by the solid circles in Figure 5, where they are compared with histograms calculated for our conventional equation of state with compressibility coefficient  $K = 200$  MeV. We have also made similar comparisons with results calculated for the other two equations of state illustrated in Figure 2.

Our calculated distributions are obtained by constructing from the velocity vectors at some large time the energy and angular distributions for the expanding matter. The small amount of matter that already has passed through the top and side boundaries of the computational mesh is also included. By integrating over the appropriate ranges of impact parameter, we compute the double-differential cross section corresponding both to all impact parameters and to central collisions constituting 15% of the total cross section. The cross section for the outgoing matter distribution is then converted into the cross section  $d^2\sigma/dE d\Omega$  for outgoing charged particles under the assumption of uniform charge density. Some measure of the fairly large numerical inaccuracies inherent in fluid dynamical calculations can be determined from the fluctuations in the histograms, which are obtained using angular bins of  $10^\circ$  width.

Examining first the results for all impact parameters given in left-hand side of Figure 5, we see that at low energy the calculated results are for all angles higher than the experimental results. This is because of our neglect of binding, which causes the entire system to completely disintegrate into slowly moving matter for an arbitrarily small impulse. At higher energy the calculations with all equations of state reproduce, to within numerical uncertainties, the experimental data at all angles. We have found that the nuclear equation of state has little effect on the single-particle-inclusive cross section  $d^2\sigma/dE d\Omega$  integrated over all impact parameters.

We turn now to the results for central collisions, which are given in the right-hand side of Figure 5 for our conventional equation of state with  $K = 200$  MeV. At intermediate angles the results calculated with the three equations of state are very similar to one another, to within numerical uncertainties. However, at  $\theta = 30^\circ$  the slope of the energy spectrum decreases significantly as we go from a stiff equation of state with  $K = 400$  MeV through an intermediate one with  $K = 200$  MeV to a soft one that contains a density isomer. Also, at  $\theta = 150^\circ$  the results calculated for the density isomer are somewhat higher than those calculated for the two conventional equations of state. These differences arise because the softer density-isomer equation of state leads to higher initial density and thermal energy per nucleon, which increases the thermal contribution to the cross section in regions where it would otherwise be small.

Because of our neglect of binding, at low energy the calculated results for central collisions are also higher than the experimental results for all angles and equations of state except for  $\theta = 150^\circ$  with the two conventional equations of state, where the rapid expansion in the backward direction suppresses the cross section. At higher energy the calculations with all equations of state reproduce, to within numerical uncertainties, the experimental data at all angles except  $\theta = 30^\circ$ , where the calculated energy spectra for all three equations of state have significantly larger slopes than the experimental spectrum. This important discrepancy for central collisions in the forward direction could arise from several different possibilities, but the most likely is that upon contact the target and projectile interpenetrate substantially. This interpenetration can be taken into account, while retaining some degree of coherent collective flow, by means of a nuclear two-fluid model, to which we now turn our attention.

### Nuclear two-fluid dynamics

In the nuclear two-fluid model coupled relativistic equations of motion are solved for separate target and projectile nuclear fluids.<sup>5,11</sup> The terms in the equations that couple the two nuclear fluids are obtained from the cross section and mean longitudinal momentum transfer for free nucleon-nucleon collisions. At low relative velocities the target and projectile fluids merge, in which case conventional relativistic nuclear fluid dynamics (which we alternatively refer to as one-fluid dynamics) is recovered.

The equations of motion for the target and projectile nuclear fluids express the conservation of nucleon number, energy, and momentum, plus the transfer of energy and momentum between the two fluids. For a given fluid, the relativistic equations of motion are analogous to Eqs. (5)-(7) for conventional nuclear fluid dynamics, but contain in addition coupling terms that describe the transfer of energy and momentum from one fluid to the other as they interpenetrate. In particular, when the relative velocity of the two fluids is large compared to the Fermi velocity of the nucleons comprising each fluid, the relativistic equations of motion for fluid 1 are<sup>5,11</sup>

$$\frac{\partial N_1}{\partial t} + \nabla \cdot (\vec{v}_1 N_1) = 0 \quad , \quad (12)$$

$$\frac{\partial \vec{M}_1}{\partial t} + \nabla \cdot (\vec{v}_1 \vec{M}_1) = -\nabla p_1 - D(\gamma_1 \vec{v}_1 - \gamma_2 \vec{v}_2) \quad , \quad (13)$$

and

$$\frac{\partial E_1}{\partial t} + \nabla \cdot (\vec{v}_1 E_1) = -\nabla \cdot (\vec{v}_1 p_1) - D(\gamma_1 - \gamma_2) \quad ; \quad (14)$$

those for fluid 2 are obtained by interchanging the subscripts 1 and 2. The drag function  $D$  involves the nucleon number densities and velocities of the two fluids, as well as the

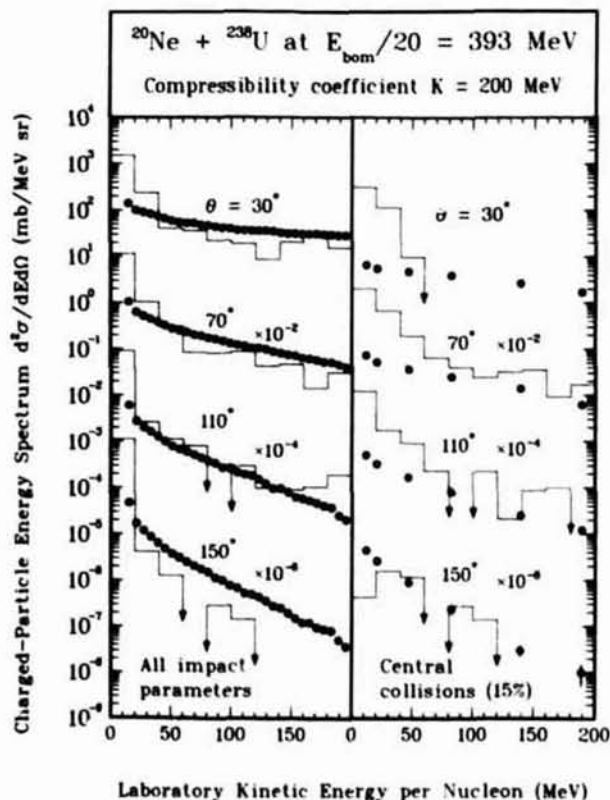


Figure 5. Comparison of calculated histograms with experimental points (Refs. 9 and 10).

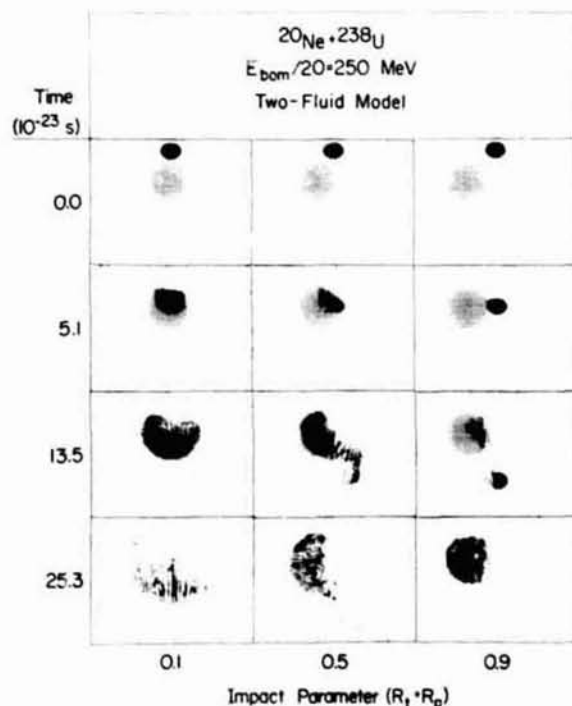


Figure 6. Time evolution of the matter distribution calculated in the two-fluid model.

cross section and average longitudinal momentum transfer for free nucleon-nucleon collisions. For the nuclear equation of state specified by Eqs. (2)-(4), these equations of motion are solved by use of a two-fluid generalization of the relativistic particle-in-cell technique.<sup>5, 8, 11</sup>

We show in Figure 6 some examples of the two-fluid solutions for the reaction  $^{20}\text{Ne} + ^{238}\text{U}$  at a laboratory bombarding energy per nucleon of 250 MeV. These results are qualitatively similar to those shown in Figure 3 for conventional nuclear fluid dynamics, especially during the later stages of the process. However, because the target and projectile interpenetrate somewhat before they begin to respond to the presence of the other, the initial compression is less and the amount of matter emerging in the backward direction is less in the two-fluid model than in conventional nuclear fluid dynamics.

Figure 7 shows the resulting energy spectra calculated for central collisions in both the one-fluid and two-fluid models with the same equation of state, along with the experimental data of Stock et al.<sup>10</sup> For the three angles  $\theta = 70^\circ, 110^\circ,$  and  $150^\circ$ , the two models reproduce equally well, to within numerical uncertainties, the experimental data at high energy and are both larger than the experimental data at low energy because of our neglect of binding. For  $\theta = 30^\circ$ , the two-fluid model agrees with the experimental data substantially better than does the one-fluid model, although the slope calculated from the two-fluid model is still somewhat larger than the experimental slope. However, as shown earlier for the one-fluid model, a softer nuclear equation of state than the one used here would increase slightly the calculated high-energy yield in forward directions.

An alternative and perhaps more illuminating way of making the comparisons for central collisions is in the form of angular distributions for fixed outgoing laboratory momentum per nucleon, as shown in Figure 8. The experimental angular distributions for low outgoing momenta contain a small peak that shifts to smaller angles and finally disappears for higher outgoing momenta. Unfortunately, this peak could be the result of either the neglect of  $^3\text{He}$ ,  $^4\text{He}$ , and heavier composite particles, whose yields are concentrated at low energies and forward directions, or the Coulomb interaction, which provides a transverse driving force for slow-moving charged particles.

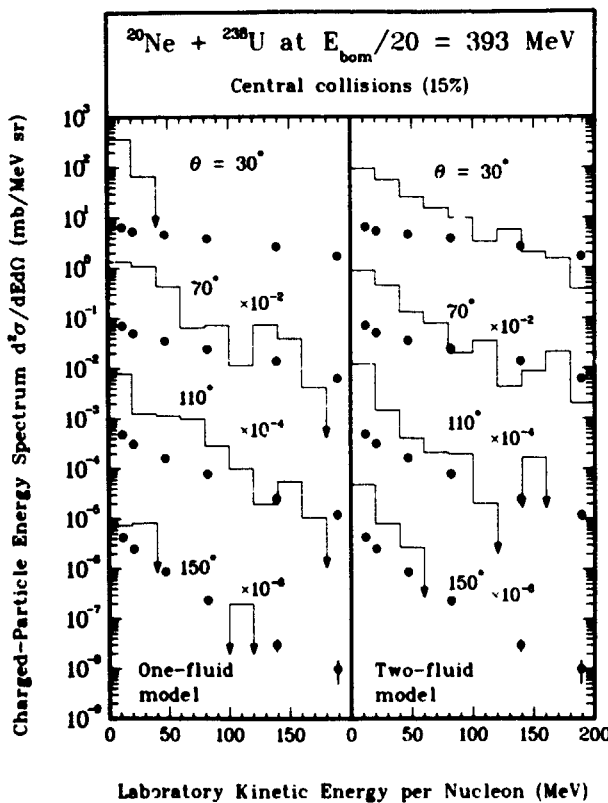


Figure 7. Comparison of calculated histograms with experimental points (Ref. 10).

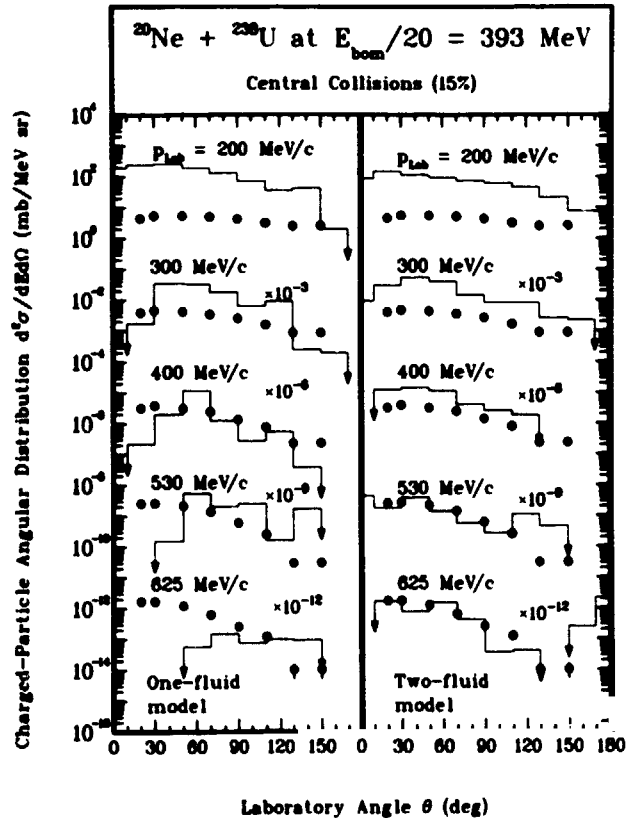


Figure 8. Comparison of calculated histograms with experimental points (Ref. 10).

The histograms are calculated with energy bins of 20 MeV. Because of our neglect of binding, the results for the lowest outgoing momentum calculated in both the one-fluid and two-fluid models are much larger than the experimental data. With increasing outgoing momentum, the one-fluid model predicts angular distributions that are narrower than the experimental distributions and that are peaked at increasingly larger angles, which is opposite to the experimental trend. However, as shown by Stöcker et al.,<sup>3</sup> the agreement between the one-fluid model and experiment would be improved by superimposing the remaining thermal energy at a freezeout density at which fluid dynamics ceases to be valid. The two-fluid model predicts angular distributions with peaks that shift to smaller angles with increasing outgoing momentum, as is observed experimentally. For intermediate outgoing momenta the experimental data are lower in absolute value than the two-fluid calculations, but for the two highest outgoing momenta the experimental data agree with the two-fluid calculations to within their numerical uncertainties. By comparison, microscopic models based on independent two-particle collisions yield for central collisions angular distributions that are essentially forward peaked at all outgoing energy.<sup>1-3</sup>

### Conclusions

With some qualifications, we conclude that in relativistic nuclear collisions the target and projectile interpenetrate substantially upon contact, but that some degree of coherent collective flow is involved. Although conventional relativistic nuclear fluid dynamics is deficient in several respects, relativistic nuclear two-fluid dynamics satisfactorily describes many aspects of relativistic nuclear collisions. Because the calculated results are not very sensitive to the input nuclear equation of state, we do not yet know whether or not there are any phase transitions as the nuclear density is increased. The answer to this question is relevant not only to atomic nuclei but also to neutron stars, illustrating once again how drops and bubbles help unify our understanding of physical systems differing in size by twenty orders of magnitude.

### Acknowledgments

We are grateful to R. Stock, Y. Yariv, Z. Fraenkel, and B. Schürmann for enlightening discussions and for providing us with their experimental data and theoretical calculations prior to publication. This work was supported by the U. S. Department of Energy.

### References

1. Yariv, Y. and Fraenkel, Z., "Intranuclear Cascade Calculation of High Energy Heavy Ion Collisions: Effect of Interactions between Cascade Particles," Phys. Rev. C, Vol. 24, pp. 488-494. 1981. Also private communication.
2. Schürmann, B. and Chemtob, M., "Direct Versus Thermal Particle Emission in High-Energy Heavy-Ion Collisions: Multiplicity-Selected Proton Inclusive Spectra," Z. Phys. A, Vol. 294, pp. 371-376. 1980. Also private communication.
3. Stöcker, H., Riedel, C., Yariv, Y., Csernai, L. P., Buchwald, G., Graebner, G., Maruhn, J. A., Greiner, W., Frankel, K., Gyulassy, M., Schürmann, B., Westfall, G. D., Stevenson, J. D., Nix, J. R., and Strottman, D., "Nuclear Fluid Dynamics versus Intranuclear Cascade--Possible Evidence for Collective Flow in Central High Energy Nuclear Collisions," Lawrence Berkeley Laboratory Preprint No. LBL-12634. 1981.
4. Gyulassy, M. and Greiner, W., "Critical Scattering and Pionic Instabilities in Heavy Ion Collisions," Ann. Phys. (N. Y.), Vol. 109, pp. 485-527. 1977.
5. Nix, J. R., "Theory of High-Energy Heavy-Ion Collisions," Prog. Part. Nucl. Phys., Vol. 2, pp. 237-284. 1979.
6. Amsden, A. A., Harlow, F. H., and Nix, J. R., "Relativistic Nuclear Fluid Dynamics," Phys. Rev. C, Vol. 15, pp. 2059-2071. 1977.
7. Nix, J. R. and Strottman, D., "Effect of a Density Isomer on High-Energy Heavy-Ion Collisions," Phys. Rev. C, Vol. 23, pp. 2548-2556. 1981.
8. Harlow, F. H., Amsden, A. A., and Nix, J. R., "Relativistic Fluid Dynamics Calculations with the Particle-in-Cell Technique," J. Comp. Phys., Vol. 20, pp. 119-129. 1976.
9. Sandoval, A., Gutbrod, H. H., Meyer, W. G., Stock, R., Lukner, C., Poskanzer, A. M., Gosset, J., Jourdain, J. C., King, C. H., King, G., Nguyen, V. S., Westfall, G. D., and Wolf, K. L., "Spectra of p, d, and t from Relativistic Nuclear Collisions," Phys. Rev. C, Vol. 21, pp. 1321-1343. 1980.
10. Stock, R., Gutbrod, H. H., Meyer, W. G., Poskanzer, A. M., Sandoval, A., Gosset, J., King, C. H., King, G., Lukner, C., Nguyen, V. S., Westfall, G. D., and Wolf, K. L., "Emission Patterns in Central and Peripheral Relativistic Heavy-Ion Collisions," Phys. Rev. Lett., Vol. 44, pp. 1243-1246. 1980. Also private communication.
11. Amsden, A. A., Goldhaber, A. S., Harlow, F. H., and Nix, J. R., "Relativistic Two-Fluid Model of Nucleus-Nucleus Collisions," Phys. Rev. C, Vol. 17, pp. 2080-2096. 1978.